The Supramolecular Chemistry of Gold and L-Cysteine: Formation of Photoluminescent, Orange-Emitting Assemblies With Multilayer Structure

*Balázs Söptei[a], Judith Mihály[a], Imola Cs. Szigyártó[a], András Wacha[a], Csaba Németh[a], Imre Bertóti[a], Zoltán May[a], Péter Baranyai[a], István E. Sajó[b], Attila Bóta[a]**

[a] Research Centre for Natural Sciences, Hungarian Academy of Sciences, 2. Magyar tudósok blvd., 1117 Budapest, Hungary

[b] Szentágothai Research Centre, University of Pécs, 20. Ifjúság road, 7624

* corresponding author; e-mail: bota.attila@ttk.mta.hu; phone: +3613826427

Abstract

The protein mediated approach is a common method for the synthesis of photoluminescent gold quantum clusters (GQCs), where proteins, acting as reducing and stabilizing agents, react with gold salts through cysteine residues. For the better understanding of the phenomenon, the aqueous phase reaction of $HAuCl_4$ and L-cysteine has been investigated at the supramolecular level by various experimental techniques and molecular mechanics simulations. We have observed the formation of a novel photoluminescent product, $(AuCys)_n^{\beta}$, which shows emission in the orange region of the spectrum. Small- and wide-angle X-ray scattering (SWAXS) measurements have revealed the presence of nanosized lamellae, which have an internal multilayer superlattice structure with a characteristic periodic distance of 1.3 nm. Based on the results, the layers are built up by zigzag shaped $(AuCys)_n$ polymer chains connected through aurophilic bonds. The aurophilic network is stabilized via salt bridges and hydrogen bonds, which are also responsible for the interlayer interactions. Here, the evolution of the multilayer structure has been monitored by the combined application of photoluminescence spectroscopy and time-resolved SAXS. It has been concluded that there is a strong correlation between the emission and the scattering intensity, which suggests that the two- and three-dimensional aggregation of the building blocks to form sheets and multilayers are simultaneous processes. Furthermore, we have revealed that the formation and behavior of $(AuCys)_n^{\beta}$ show significant differences to that of Au-L-glutathione compounds desrcibed earlier despite the similarity of L-cysteine and L-glutathione. These results evidence that L-cysteine and gold species form building blocks that can be applied expansively in supramolecular and cluster chemistry.

Keywords

photoluminescence, self-assembly, aurophilicity, supramolecular chemistry, gold clusters, multilamellar nanostructures

1. Introduction

Supramolecular assemblies of gold complexes show intriguing features that can be exploited in various application fields. Photoluminescence is the most spectacular attribute of these materials. Products emitting in the visible range of the spectrum can be applied in fields of analytics, sensorics and photoluminescence imaging. A family of luminescent gold assemblies, commonly referred as Gold Quantum Clusters (GQCs), has recently gained serious attention [1-4]. In order to achieve stable, biocompatible products with a hydrophilic character, biomolecules such as peptides and proteins are often used as reducing agents and stabilizing ligands in gold quantum cluster preparation methods.[4] In a previous study, we have investigated the role of different amino acid residues in the protein-mediated synthesis of red-emitting GQCs. Tyrosine and cysteine residues of the biomolecules have been found to have an exceptional function in the process [5]. In a further research phase, we have examined the role of L-cysteine (Cys) in the supramolecular chemistry of gold.

It is known that cysteine residues reduce Au^{3+} to form Au^{+} species [6,7], which is a critical step in the formation of photoluminescent products [8,9]. Recently, the chemistry of gold and biogenic thiols (including Cys) has been investigated at the molecular level. Thiols have been found to react with Au^{3+} through substitution and reduction processes [10].

$$[Au(H_2O)_3Cl]^{2+} + RSH + H_2O \rightarrow [Au(H_2O)_3SR]^{2+} + H_3O^{+} + Cl^{-}$$

Abbreviations

$(AuCys)_n$, Au-(L-cysteine) polymer; $(AuCys)_n^{\alpha}$, non-luminescent aggregate of Au-(L-cysteine) polymers; $(AuCys)_n^{\beta}$, photolumiescent supramolecular product of Au-(L-cysteine) polymers; Cys, L-cysteine; GSG, L-glutathione; GQC, gold quantum cluster; FFTEM, freeze fracture transmission electron microscopy; FTIR, Fourier-transform infrared; ICP-OES, inductively coupled plasma optical emission spectrometry; SWAXS, small- and wide- angle X-ray scattering; XPS, X-ray photoelectron spectroscopy;

$[Au(H_2O)_3SR]^{2+} + RSH \rightarrow [Au(H_2O)_2]^{+} + (RS)_2 + H_3O^{+}$

The outcome of the reaction is determined by the stoichiometry of the reactants. If the thiol is present in excess, Au^{+} species can be stabilized as Au^{+}-thiolate complexes [10]. In a further step, oligo- and polymeric compounds form [11,12].

$[Au(H_2O)_2]^{+} + RSH \rightarrow [Au(H_2O)SR] + H_3O^{+}$

$n[Au(H_2O)SR] \rightarrow (AuSR)_n + nH_2O$

The $(AuSR)_n$ species can aggregate through intermolecular interactions, which results in the formation of various photoluminescent assemblies [8, 14-16].

At high pH values, the behavior of proteins and peptides with cysteine and tyrosine residues is analogous to that of thiols. The ratio of the precursors is an important factor in the reaction. At high biomolecule:Au ratios, gold quantum clusters form. Nanoparticles are produced if the ratio of the reactants is low [5,17,18]. This suggests that Cys can mediate the formation of photoluminescent gold species under certain conditions. Furthermore, the investigation of the reaction of Cys and gold salts can brings us closer to the understanding of protein- and peptide-based formation of gold quantum clusters. Despite all these, the supramolecular chemistry of Au-Cys compounds has not been studied until now. Here, we report the preparation of a novel supramolecular nanostructure with orange emission, and also the analysis of the formation mechanism.

2. Materials and methods

2.1. Materials

$HAuCl_4$ (99.999 %), sodium borohydride (99.99%), and thioglycolic acid (≥99%) were ordered from Aldrich. L-cysteine (BioUltra, ≥98.5%) and th ioglycerol (≥99.0%) were purchased from Sigma. Deionized water of Millipore purity (18.2 MW cm) was used in all experiments.

2.2. Preparation of supramolecular gold-L-cysteine assemblies

Supramolecular assemblies were prepared via an aqueous phase method. Aliquots of $HAuCl_4$ (10^{-2} M) and L-cysteine (10^{-1} M) solutions in avolume ratio of 1:1 were mixed. A yellow precipitate

formed, which was washed with excess water after removing the supernatant. After resuspending in deionized water, samples were incubated at 25°C, 50°C, and 75°C, respectively. Emission spectra were recorded at different time points in the time range between 0 to 8 hours.

2.3. UV-Vis and photoluminescence (PL) spectroscopy

An Agilent 8453 spectrophotometer was applied for the collection of UV-Vis spectra. An Edinburgh Instruments FLSP920 luminescence spectrometer was used for the steady-state and time-resolved photoluminescence measurements. Samples were excited at 378 nm. Quantum yield of the product has been determined using cresyl violet as a reference.

2.4. Fourier-transform infrared (FTIR) spectroscopy

FTIR spectra were collected in attenuated total reflection (ATR) mode. A Varian FTS-2000 FTIR Spectrometer (Varian Inc., USA) with a Golden Gate single reflection diamond ATR (SPECAC Ltd., UK) accessory was used. Aliquots of the samples (5 μL) were spread on the ATR crystal. 128 scans at a resolution of 2 cm^{-1} were co-added.

2.5. X-ray photoelectron spectroscopy (XPS)

Spectra were recorded using a Kratos XSAM 800 spectrometer using Mg $K\alpha_{1,2}$ (1253.6 eV) excitation. Quantitative analysis was performed with the Kratos Vision 2 and by the XPS MultiQuant programs [19,20].

2.6. Inductively Coupled Plasma Optical Emission Spectrometry (ICP-OES)

The determination of the gold:sulphur ratio was carried out using a Spectro Genesis simultaneous spectrometer with axial plasma viewing. Before the measurements, aqua regia was added to the samples, which were boiled for 1-2 hours to dissolve gold completely.

2.7. Small- and wide-angle X-ray scattering (SWAXS)

Experiments were performed on CREDO, a new SAXS instrument constructed by our research group [21]. Highly monochromatic Cu Kα radiation was generated using a $GeniX^{3D}$ Cu ULD integrated beam delivery system (Xenocs SA, Sassenage, France), which consists of a 30 W

microfocus X-ray tube and an integrated parabolic multilayer mirror. Scattered X-rays were detected by a Pilatus-300k CMOS hybrid pixel detector (Dectris Ltd, Baden, Switzerland).

2.8. Freeze Fracture Transmission Electron Microscopy (FFTEM)

1 μL aliquots were pipetted onto gold sample holders and frozen in partially solidified Freon and stored in liquid nitrogen. Fracturing was performed at −100 °C with a Balzers freeze fracture device (Balzers BAF 400D, Balzers AG, Vaduz, Liechtenstein). A platinum−carbon shadowing was applied. The replicas were placed on 200-mesh copper grids. A Morgagni 268D (FEI, USA) transmission electron microscope was used for the imaging.

3. Theory/Calculation

Molecular mechanics simulations were carried out using ChemBio3D Ultra. $(AuCys)_5$ oligomer blocks were constructed in order to obtain the optimal set of conditions regarding the edge effects and the calculation time. The behavior of $(AuCys)_5$ molecules has been studied in aqueous phase. H_2O molecules were placed randomly in the environment of the oligomer chains. Alignment of the oligomer chains has been investigated via energy minimization using two approaches: with and without the introduction of aurophilicity.

4. Results and Discussion

The reaction of Cys and $HAuCl_4$ has intriguing aspects beyond the molecular level. At amino acid to gold ratios not less than 1, a yellow, non-luminescent precipitate, which will be referred as $(AuCys)_n^{\alpha}$, appears rapidly after mixing the reactants. It can be dissolved easily at pH values over 12, and reacted with strong reducing agents such as $NaBH_4$ in order to obtain gold nanoparticles. After incubation, $(AuCys)_n^{\alpha}$ spontaneously transforms into an orange emitting product, which will be referred as $(AuCys)_n^{\beta}$. $(AuCys)_n^{\beta}$ forms a highly stable, opalescent suspension in aqueous medium. The light scattering and colloidal properties of the suspension indicate that the size of the product is in the range of nanometers. Based on our experience, the formation of $(AuCys)_n^{\beta}$ takes place in a wide pH and temperature range (Figure S1). The ratio of the reactants, on the other hand,

is a crucial factor. If the Cys:Au ratio is less than 1, a purple/brown precipitate is formed, indicating the presence of aggregated gold nano- or microparticles. It is known that the reactivity of $[Au(H_2O)_2]^+$ complexes is much higher than that of Au^I-thiolates. Furthermore, the substitution of H_2O ligands with O- and N-donor ligands is not favoured [11,22]. Therefore, a spontaneous disproportionation of Au^+ takes place in the absence of free thiol groups. Thus, the stoichiometry-dependent behavior of proteins and peptides in the reaction with gold salts can be explained through the thiol complex formation of Au^+ species.

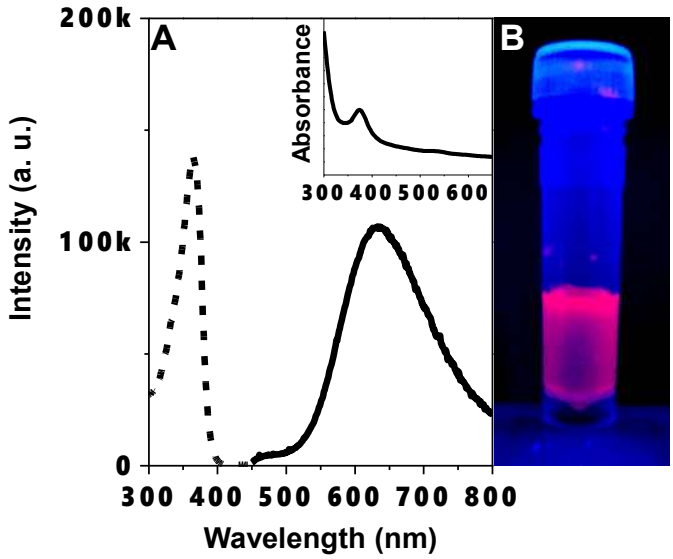

Figure 1. (A) Emission (solid) and excitation (dashed) spectrum of $(AuCys)_n^{\beta}$. Inset shows UV-Vis spectrum of the product. (B) Aqueous suspension of $(AuCys)_n^{\beta}$ - photography under UV lamp (excited at 365 nm).

$(AuCys)_n^{\beta}$ shows visible emission in the orange region at 630 nm (see Figure 1A). Luminescence properties can be detected via examination of the incubated samples under UV light (Figure 1B). In contrast to the Au-L-glutathione (Au-GSH) system [15], the incubation temperature did not have a significant effect on the emission wavelength (Table 1).

Table 1. Emission wavelength of $(AuCys)_n^{\beta}$ samples with different incubation time and temperature values.

Incubation time (s)	Incubation temperature (°C)		
	75	*50*	*25*
2400	632 (±1)	628 (±1)	-
3600	634 (±1)	631 (±1)	628 (±1)
7200	632 (±1)	632 (±1)	629 (±1)
14400	632 (±1)	631 (±1)	633 (±1)
28800	632 (±1)	631 (±1)	634 (±1)

An excitation peak, along with an UV-Vis absorption peak, is located at approximately 360 nm, which is a characteristic transition of supramolecular gold compounds and gold clusters [14-16]. The absence of plasmon absorption peaks indicated that the formation of gold nanoparticle byproducts can be ruled out [23]. Photoluminescence lifetime of the samples has been estimated, values in the range of microseconds have been obtained (τ_1 = 0.7 μs with α_1 = 0.52, and τ_2 = 2.4 μs with α_2 = 0.48). This is in correspondence with the characteristic emission lifetime values of GQCs and Au^+-phenylthiolate assemblies reported earlier [5,14,24-26]. A quantum yield value of 1.1% has been estimated for $(AuCys)_n^{\beta}$, which is in the same order of magnitude than that of BSA-protected gold quantum clusters [6]. However, the obtained value is probably lower than the actual quantum yield of $(AuCys)_n^{\beta}$, since the light scattering of the product results in an increase in the measured absorbance.

The chemical composition of $(AuCys)_n^{\beta}$ has been investigated. Comparison of the binding energies (BE) of native L-cysteine and the synthesized $(AuCys)_n^{\beta}$ samples via XPS showed that sulfur possesses lower BE in $(AuCys)_n^{\beta}$ samples (Figure S2). The significant, 0.6 eV shift manifests the S-Au bonding in the $(AuCys)_n^{\beta}$, with a charge transfer from Au to S. The bond between gold and sulfur, however, has been shown to have a covalent character [27]. The BE of gold in $(AuCys)_n^{\beta}$ was found to be close to that of gold nanoparticles (see Figure S3), which is intriguing because the formal oxidation state of gold in gold-thiolate polymers has been reported to be +1. The behavior of the product, however, suggests that the oxidation state of gold is above zero: $(AuCys)_n^{\beta}$ reacts with

sodium borohydride: the emission vanishes, and a purple precipitate is formed (see Figure S4). Thus, we can assume that the average oxidation state of the gold in $(AuCys)_n^{\beta}$ is a value between 0 and +1. The apparent quasi-metallic chemical state of gold in $(AuCys)_n^{\beta}$ might be the consequence of the aggregation of multiple gold atoms creating an extended Au-Au bonding system, stabilized by the cysteine molecules.

Quantitative XPS results indicated an Au:Cys ratio very close to a 1:1 stoichiometry in $(AuCys)_n^{\beta}$ (see Figure S5). The same ratio has been determined by the ICP-OES method. This ratio of gold atoms and the ligand molecules is characteristic of several Au^+-thiolate compounds reported earlier in the literature, e. g. gold sodium thiomalate (also known as myochrysine) and Au^+-phenylthiolate [14,28]. The $(AuCys)_n^{\beta}$ product, however, shows emission properties quite similar to that of the latter, which suggests a structural analogy between the two systems. According to the literature, the $(AuRS)_n$ polymers are held together by bridging thiol groups [11]. The composition of such products is in correspondence with our results.

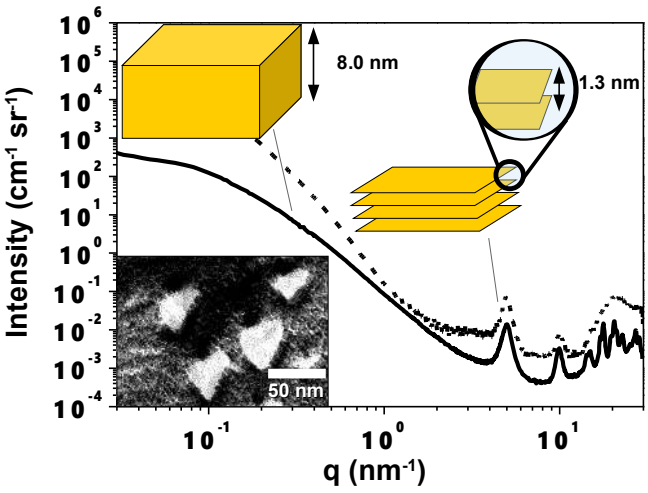

Figure 2. Small- and wide-angle X-ray scattering (SWAXS) curve of $(AuCys)_n^{\beta}$ suspension (dashed line) and powder (solid line) with calculated characteristic distances. Inset shows freeze fracture transmission electron microscopy (FFTEM) image of $(AuCys)_n^{\beta}$.

The SWAXS method was applied in order to gain information on the size and morphology of the product. In the SWAXS patterns of $(AuCys)_n^{\beta}$, shown in Figure 2, a characteristic peak can be detected at a q value of 5 nm^{-1}, which corresponds to a multilayer superlattice structure with a periodic distance of 1.3 nm. This peak does not manifest itself in the $(AuCys)_n^{\alpha}$ intermediate (see Figure S4), suggesting that photoluminescence of $(AuCys)_n^{\beta}$ is related to this structural motif. The layers are detectable both in the dry powder and in the aqueous suspension of $(AuCys)_n^{\beta}$, first and second orders of the peaks are clearly observable. The peak positions in the two states show only slight differences, indicating that the layered structure of $(AuCys)_n^{\beta}$ is preserved in the absence of water. This might be a consequence of the rigidity of the ligand molecules. In the case of GSH, which is a more flexible ligand, hydrogel nature of the assemblies has been observed [29]. In contrast to this, $(AuCys)_n^{\beta}$ shows a nanoparticle-like behavior.

The low-q scattering of particulate systems is characterized by the so-called Guinier approximation, i. e. the scattering curve can be described by the following function:

$$I(q \approx 0) = I_0 e^{\frac{-q^2 R_g^2}{3}},$$

where I_0 is the extrapolated value of the scattered intensity at zero scattering angle (also called the forward scattering) and R_g is the radius of gyration, a quantity describing an average linear dimension of the scatterer objects – particles, proteins, etc.

After the Guinier region, the so-called Fourier range is found, which characterize the shape of the scatterers. The small-angle scattering pattern of particulate systems ends with the Porod region, where the scattering curve can be approximated with a negative power q, the exponent describing the roughness of the surface of the particles.

In the special case of lamellar particles, i. e. when one dimension of the scattering objects is much smaller than the other two, scattering in the Fourier region can be described by the formula

$$I_{lamella} = G q^{-2} e^{-q^2 R_t^2},$$

where R_t is a radius of gyration-like quantity describing the thickness of the lamellae and G is a scaling factor. This function is formally very similar to the Guinier approach, thus a generalized version can be written:

$$I = G q^{3-s} e^{\frac{-q^2 R_{g,s}^2}{n}},$$

where n is the dimensionality of the quantity of which the radius of gyration is to be determined: in the lamellar case n=1, since we are dealing with a thickness. In the traditional Guinier case n=3 since the radius of gyration of a three-dimensional object has to be found, and case n=2 corresponds to the cross-section of infinitely long columns.

B. Hammouda introduced an empirical model to unify Guinier-like and power-law scattering by constraints of continuity in the curve and its first derivative [30]. In the case of $(AuCys)_n^{\beta}$, the curve starts with a q^{-2} power-law, which later turns down, indicating a case for lamellae. At larger angles another power-law can be found. Our fitting function therefore looks as

$$I(q) = C + \begin{cases} G q^{3-n} e^{-q^2 R_{g,s}^2} & if \quad q < q^{\times} \\ A q^{\alpha} & otherwise \end{cases},$$

The thickness of the lamellae can be calculated as

$$T = \sqrt{12}\, R_{g,1}$$

From the slope of the curves in the region of small angles, the presence of nanometer-sized sheets with an estimated thickness of 8 nm can be deduced (see Figure S7). FFTEM has been applied to visualize the products (see inset in Figure 2). Flat entities with a thickness of several nanometers have been observed, which is in accordance with the SAXS results. Peaks corresponding to distances close to 0.3 nm can be detected in the SWAXS curves of the dry samples, which are characteristic of the aurophilic bonds [8,9,31].

The formation of supperlattices is a feature of gold compounds. The phenomenon has been reported in several cases including the case of bovine serum albumin coated GQCs in lipids, Au^+-thiobarbiturate, and Au-GSH species [11,29,32]. Regarding the latter, it has been concluded that the

layers consist of hexagonally arranged gold and sulfur atoms with arrays of the peptide ligands bulging perpendicularly to the plane [29]. In other works on Au-thiolates such as Au-thiomalate or Au-phenylthiolate, zigzag shaped chains of the polymers with and alternating arrangement of ligand molecules have been proposed [13,32,33]. Luminescent gold(I) acetylides with the same shape have been reported [34]. Since Cys is related to GSH, we have examined both the hexagonal and the zigzag chain form of $(AuCys)_n^{\beta}$ via molecular mechanics. Results have shown that in the former case, the average interlayer distance between the hexagonal layers is approximately 1.0 nm on average (see Figure S8). Assuming that the layers are built up by zigzag polymers held together via aurophilic bonds (Figure 3), an interlayer distance of 1.3 nm has been obtained, which matches the characteristic distance measured via the SAXS method. Thus, we can conclude that the zigzag chain arrangement is a more realistic approximation for the structure of $(AuCys)_n^{\beta}$. It is worth noting that the presence of intra- and interlayer hydrogen bonds can be observed, which are responsible for the arrangement of ligand molecules. This is analogous to the formation of cysteine networks on Au(111) surfaces [35]. Furthermore, hydrogen bonds also play an important role in the stabilization of the aurophilic assemblies. In the case of proteins and peptides, the peptide backbone is responsible for a similar effect. The formation of long polymer chains, however, is limited due to steric conditions.

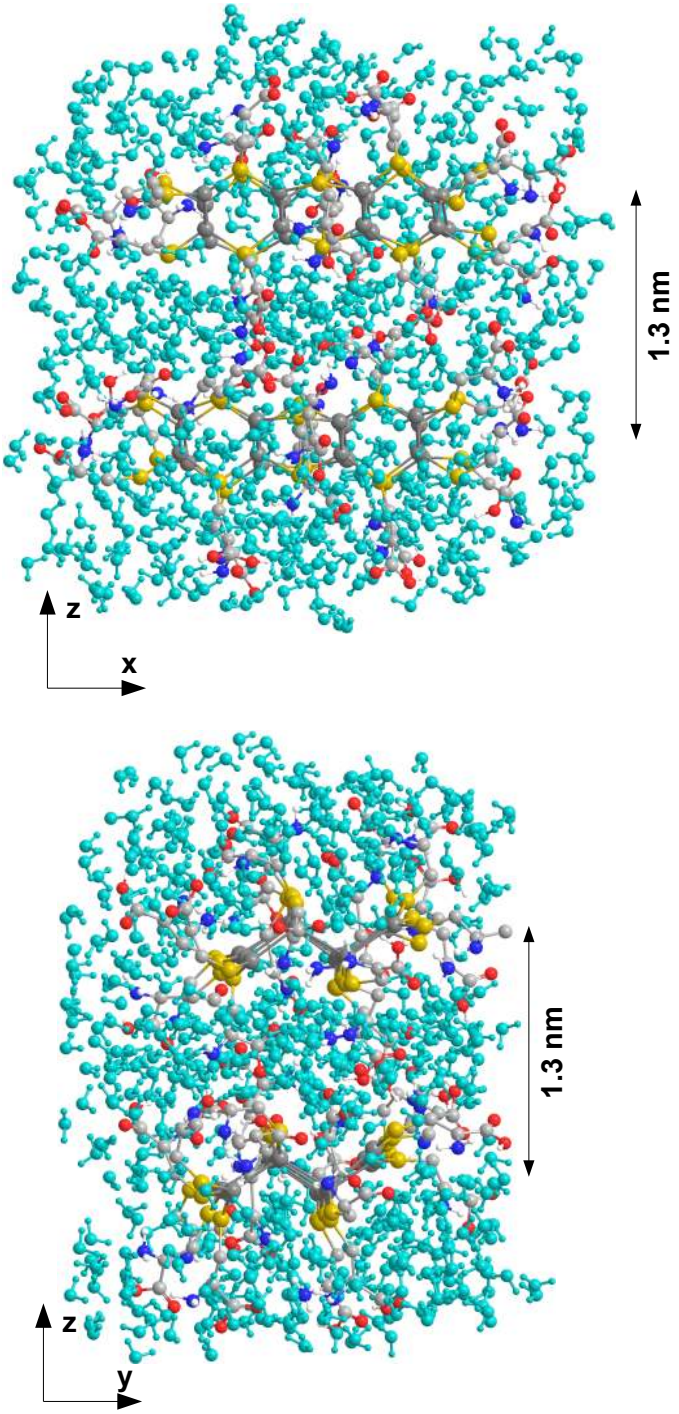

Figure 3. The proposed multilayer structure of $(AuCys)_n^{\beta}$, optimized in water via molecular mechanics. Water molecules are shown in cyan. Atoms of $(AuCys)_n^{\beta}$ are shown in different colors: dark grey, Au; yellow, S; blue N; red, O; light grey, C.

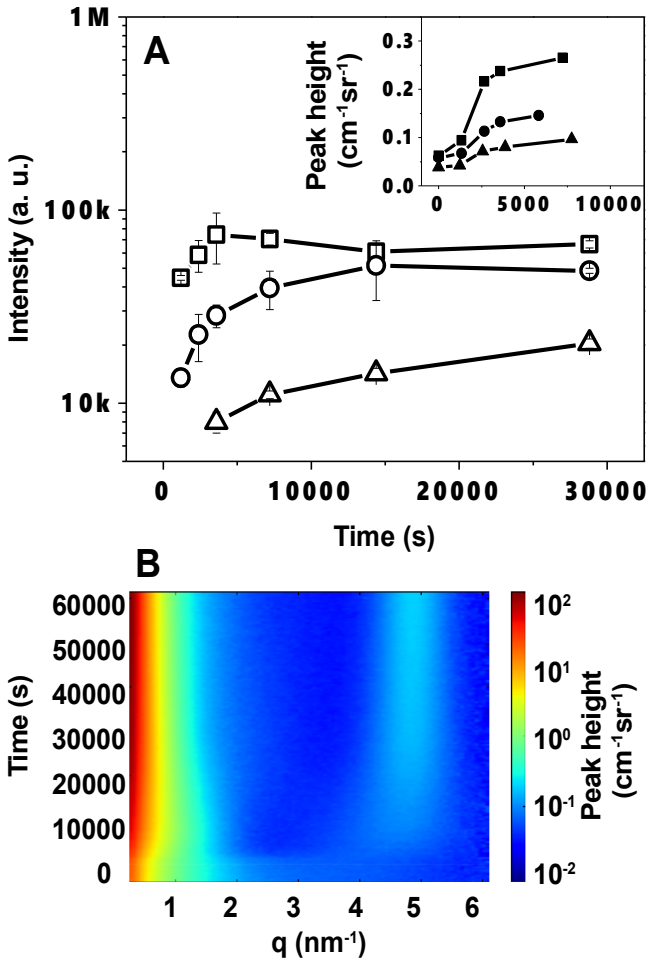

Figure 4. The formation of $(AuCys)_n^{\beta}$. (A) Photoluminescence intensity measured after incubation of the precursor at 25°C (triangles), 50°C (circles) and 75°C (squares). Inset shows the intensity of the $5nm^{-1}$ peak corresponding to the multilayer structure measured via time-resolved SAXS.[1] (B) Two-dimensional plot of the SAXS spectra measured at 25°C.

We have studied the $(AuCys)_n^{\alpha} \rightarrow (AuCys)_n^{\beta}$ transformation via photoluminescence spectroscopy and time-resolved SAXS, shown in Figure 4. At 25°C, photoluminescence reaches a saturation after eight hours of incubation. As the temperature increases, rapid formation of $(AuCys)_n^{\beta}$ can be

1 Investigation of the samples via time-resolved SAXS for longer time periods at high temperatures is problematic due to the fragilty of the borosilicate capillaries.

observed, and higher intensity values can be achieved. At 50°C, saturation is reached in less than four hours, and at 75°C, the highest emission intensity can be observed within two hours, suggesting an optimal set of parameters. In the latter case, however, a slow decomposition of the product takes place. SAXS patterns obtained at different time points show a tendency similar to that of the corresponding curves obtained by photoluminescence spectroscopy: the X-ray scattering peak appears and its intensity increases in line with the emission intensity. Based on the acquired data, the calculated correlation coefficient is 0.9208. This suggests a strong positive correlation between the multilayer structure and the emission properties. It is known that the source of the photoluminescence is the aurophilic network [8,9]. Here, the netwok is located within the layers. Thus, it is a reasonable question how this correlation occurs. In order to obtain an answer for this, we have applied molecular mechanics.

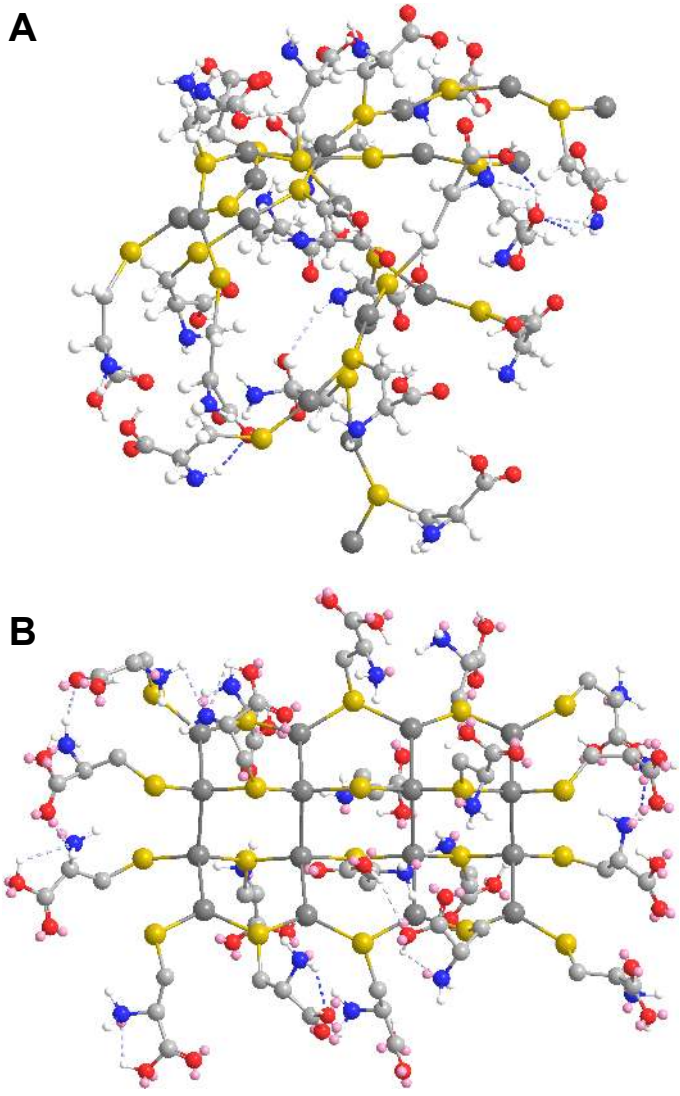

Figure 5. The alignment of $(AuCys)_5$ oligomer chains in water (A) in the absence of Au-Au bonds; (B) in the presence of Au-Au bonds. Atoms are shown in different colors: dark grey, Au; yellow, S; blue N; red, O; light grey, C; white, H. Dashed lines represent hydrogen bonds. Water molecules are omitted for clarity.

Simulations have pointed out that the aggregation of $(AuCys)_n$ chains is favoured in aqueous phase due to the formation of hydrogen bonds. This is a reasonable explanation for the low solubility of the product. Without the introduction of Au-Au bonds, however, a randomly arranged network, shown in Figure 5A, can be observed instead of the multilayer structure. It is presumable that this corresponds to the non-luminescent $(AuCys)_n^{\alpha}$ form. Layers can only form in the presence of aurophilic interaction, as shown in Figure 5B. The process also requires the breakage of hydrogen bonds and the formation of new ones, which is ensured by the motion of the polymer chains and the ligand molecules. Hydrogen bonds support the aurophilic network, leading to increased stability and rigidity of the structure. It can also be concluded that the packing of the forming layers is inevitable due to the large number of binding sites (approximately 37 amino and carboxyl groups per nm^2). Thus, the formation of the single and the multilayer structures takes place simultaneously. This resolves the apparent contradiction arising from the results of photoluminescence and time-resolved SAXS measurements.

The spontaneous nature of the self-assembly is a consequence of the molecular structure of Cys. With only a single amino and a single carboxyl groups in a ligand molecule, the uniformity of the interlayer cysteine bridges is ensured. In the case of GSH, there number of permutations is much higher. Therefore, the spontaneous formation of a highly ordered structures is not favoured. According to the literature, aggregation induced emission of Au-GSH can be observed in the presence of aggregating agents, such as ethanol or Cd^{2+} ions [15]. This is an additional difference between the two systems.

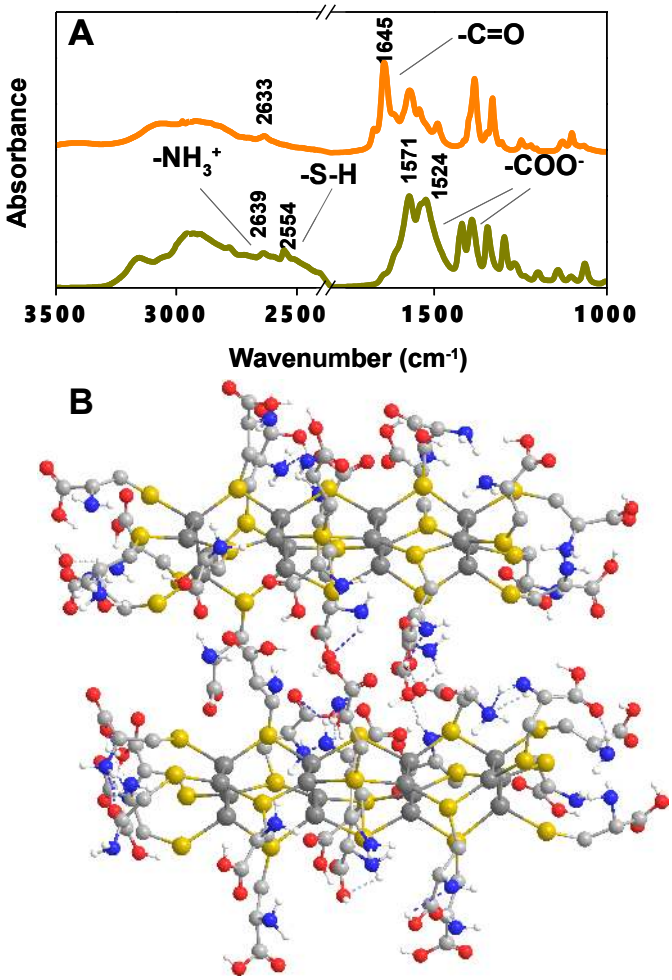

Figure 6. (A) Fourier-transform infrared (FTIR) spectrum of $(AuCys)_n^{\beta}$ (orange) and L-cysteine (green). (B) Intra- and interlayer hydrogen bonds, shown by dashed lines, in the optimized structure of $(AuCys)_n^{\beta}$.

The hydrogen bonds predicted via simulations have been detected by FTIR spectroscopy. It is known that in L-cysteine is in a zwitterionic form in a wide pH range [36]. The charged state of the amino and carboxyl groups can be observed in the FTIR spectrum: FTIR bands of the NH_3^+ groups can be observed in the range of 2630 to 2650 cm^{-1}, and that of the COO^- groups are detectable between 1500 and 1600 cm^{-1} [37]. In the FITR spectrum of $(AuCys)_n^{\beta}$, shown in Figure 6A, an additional strong band appears at 1645 cm^{-1}, which can be assigned to strongly hydrogen bonded

carbonyl νC=O vibrations [37,38,40]. This leads to the conclusion that the ligand molecules in $(AuCys)_n^{\beta}$ show a mixed behavior. There are non-dissociated amino and carboxyl groups which are hydrogen bonded, but there are also functional groups in the ionic form. This is a consequence of the distortion of the electronic structure in Cys, which takes place due to the formation of the S-Au bond. The latter, however, can be detected indirectly via FTIR spectroscopy: the band corresponding to the S-H vibrations is observable in the spectrum of L-Cys at 2554 cm^{-1} [37-39], but it is absent in the case of $(AuCys)_n^{\beta}$. Based on the molecular mechanics simulations, we can assume that both interlayer cysteine bridges are present in the product due to concomitant hydrogen bonds and electrostatic interaction (Figure 6B), resulting in the stabilization of the aurophilic assemblies. Salt bridges, however, are responsible for the self-assembly of gold nanoparticles in the presence of L-cysteine [41]. It is also worth noting that in the experiments with thioglycolic acid and thioglycerol the formation of orange-emitting products was negligible (see Figure S9), which emphasizes the importance of amino groups in the stabilization of the supramolecular structure.

5. Conclusions

The physico-chemical characterization and molecular mechanics simulations can provide the exploration of the peculiar properties of a novel photoluminescent product, $(AuCys)_n^{\beta}$, which has a multilayer superlattice structure with a characteristic periodic distance of 1.3 nm. Especially, the X-ray scattering, extended from the small to wide angle regime, is appropriate to reveal the structural characters which appear in both the atomic and nanometer levels. We have observed a well-ordered aurophilic networks of zigzag shaped (AuCys)n polymers instead of the earlier proposed hexagonal sheets of S and Au atoms in the case of Au-GSH hydrogels.

The orange emitting $(AuCys)_n^{\beta}$ is a promising nanomaterial for further, mild reduction based strategies in the development of novel biocompatible, hydrophilic GQCs. In contrast to the ethanol- or Cd^{2+}-induced formation of luminescent Au-GSH aggregates, the photoluminescent $(AuCys)_n^{\beta}$

product forms simultaneously. Furthermore, unlike the former, $(AuCys)_n^{\beta}$ shows a nanoparticle-like colloidal behavior independent of the pH of the system. These observations point out that differences in the molecular properties of the ligands, such as the rigidity and the number of hydrogen bond donors and acceptors, lead to major differences in the supramolecular behavior of the corresponding gold compounds.

By the combined application of photoluminescence spectroscopy and time-resolved small-angle X-ray scattering, a strong correlation was found between the presence of the multilayer structure and the photoluminescence emission. Molecular mechanics simulations have revealed that the correlation is a consequence of the simultaneous aggregation of $(AuCys)_n$ chains at the single- and the multilayer level. Both the 2D and 3D structures are stabilized via hydrogen bonds and salt bridges between amino and carboxyl groups, which are responsible for the intra- and interlayer interactions. Thus, the combination of photoluminescence spectroscopy and SAXS can provide information on the supramolecular processes in the case of gold compounds. Moreover, our results suggests that the fine-tuning of the optical properties can be achieved by engineering the nanostructure.

ASSOCIATED CONTENT

Supporting Information. Supporting Information Available: detaild experimental and theoretical methods, additional experimental results of XPS, PL spectroscopy, and SWAXS measurements, additional results of simulations. This material is available free of charge via the Internet at http://pubs.acs.org.

6. Contributors

The manuscript was written through contributions of all authors. All authors have given approval to the final version of the manuscript.

7. Acknowledgements

This work was supported by the Hungarian Scientific Research Fund (OTKA, Hungary) and the National Innovation Office (NIH, Hungary) under Grant Agreement CNK-81056. The authors thank Teréz Kiss for the FFTEM investigations.

8. REFERENCES

[1] Cui, M.; Zhao, Y.; Song, Q. Synthesis, Optical Properties and Applications of Ultra-Small Luminescent Gold Nanoclusters. Trends Anal. Chem. 2014, 57, 73–82.

[2] Shang, L.; Nienhaus, G. U. Gold Nanoclusters as Novel Optical Probes for in vitro and in vivo Fluorescence Imaging. Biophys. Rev. 2012, 4, 313–322.

[3] Shang, L.; Dong, S.; Nienhaus, G. U. Ultra-Small Fluorescent Metal Nanoclusters: Synthesis and Biological Applications. Nano Today 2011, 6, 401—418.

[4] Chevrier, D. M.; Chatt, A.; Zhang, P. Properties and Applications of Protein-Stabilized Fluorescent Gold Nanoclusters: Short Review. J. Nanophotonics 2012, DOI: 10.1117/1.JNP.6.064504

[5] Söptei, B.; Naszályi Nagy, L.; Baranyai, P.; Szabó, I.; Mező, G.; Hudecz, F.; Bóta, A. On the Selection and Design of Proteins and Peptide Derivatives for the Production of Photoluminescent, Red-Emitting Gold Quantum Clusters. Gold Bull. 2013, 46, 195–203.

[6] Xie, J.; Zheng, Y.; Ying, J. Y. Protein-directed Synthesis of Highly Fluorescent Gold Nanoclusters. J. Am. Chem. Soc. 2009, 131, 888–889.

[7] Glišić, B. Đ.; Rychlewska, U.; Djuran, M. I. Reactions and Structural Characterization of Gold(III) Complexes with Amino Acids, Peptides and Proteins. Dalton Trans. 2012, 41, 6887–6901.

[8] Schmidbaur, H.; Schier, A. Aurophilic Interactions as a Subject of Current Research: an Up-date. Chem. Soc. Rev. 2012, 41, 370–412.

[9] Schmidbaur, H. The Aurophilicity Phenomenon: A Decade of Experimental Findings, Theoretical Concepts and Emerging Applications. Gold Bull. 2000, 33, 3-10.

[10] Đurović, M. D.; Bugarčić, Ž. D.; Heinemann, F. W.; van Eldik, R. Substitution Versus Redox Reactions of Gold(III) Complexes with L-Cysteine, L-Methionine and Glutathione. Dalton Trans. 2014, 43, 3911-3921.

[11] Puddephatt, R. J. The Chemistry of Gold; Elsevier Scientific Publishing Company, Amsterdam, The Netherlands, 1978.

[12] Barngrover, B. M.; Aikens, C. M. Electron and Hydride Addition to Gold(I) Thiolate Oligomers: Implications for Gold-Thiolate Nanoparticle Growth Mechanisms. J. Phys. Chem. Lett. 2011, 2, 990–994.

[13] Hunks, W. J.; Jennings, M. C.; Puddephatt, R. J. Supramolecular Gold(I) Thiobarbiturate Chemistry: Combining Aurophilicity and Hydrogen Bonding to Make Polymers, Sheets, and Networks. Inorg. Chem. 2002, 41, 4590-4598.

[14] Bachman, R. E.; Bodolosky-Bettis, S. A.; Glennon, S. C.; Sirchio, S. A. Formation of a Novel Luminescent Form of Gold(I) Phenylthiolate via Self-Assembly and Decomposition of Isonitrilegold(I) Phenylthiolate Complexes. J. Am. Chem. Soc. 2000, 122, 7146-7147.

[15] Luo, Z.; Yuan, X.; Yu, Y.; Zhang, Q.; Leong, D. T.; Lee, J. Y.; Xie, J. From Aggregation-Induced Emission of Au(I)−Thiolate Complexes to Ultrabright Au(0)@Au(I)−Thiolate Core−Shell Nanoclusters. J. Am. Chem. Soc. 2012, 134, 16662−16670.

[16] Park, S., Y.; Lee, D.Synthesis and Electrochemical and Spectroscopic Characterization of Biicosahedral Au_{25} Clusters. Langmuir 2012, 28, 7049−7054.

[17] Xavier, P. L.; Chaudhari, K.; Verma, P. K.; Pal, S. K.; Pradeep, T. Luminescent quantum clusters of gold in transferrin family protein, lactoferrin exhibiting FRET. Nanoscale 2010, 2, 2769–2776.

[18] Wei, H.; Wang, Z.; Yang, L.; Tian, S.; Hou, C.; Lu, Y. Lysozyme Stabilized Gold Fluorescent Cluster: Synthesis and Application as Hg^{2+} Sensor. Analyst 2010, 135, 1406–1410.

[19] Mohai, M. XPS MultiQuant: multimodel XPS quantification software. Surf. Interface Anal. 2004, 36, 828-832.

[20] Mohai, M.; Bertóti, I. Calculation of overlayer thickness on curved surfaces based on XPS intensities. Surf. Interface Anal. 2004, 36, 805-808.

[21] Wacha, A.; Varga, Z.; Bóta, A. CREDO: a new general-purpose laboratory instrument for small-angle X-ray scattering. J. Appl. Cryst. 2014, 47, 1749-1754. doi:10.1107/S1600576714019918

[22] Vicente, J.; Chicote, M. T.; Abrisqueta, M. D.; González-Herrero, P.; Guerrero, R. Recent Advances in the Chemistry of Gold(I) Complexes with C-, N- and S-Donor Ligands Part I: Alkynyl, Amino, Imino and Nitrido Derivatives. Gold Bulletin 1998, 31, 83-87.

[23] Jain, P. K.; Lee, K. S.; El-Sayed, I. H.; El-Sayed, M. A. Calculated Absorption and Scattering Properties of Gold Nanoparticles of Different Size, Shape, and Composition: Applications in Biological Imaging and Biomedicine. J. Phys. Chem. B 2006, 110, 7238–7248.

[24] Link, S.; Beevy, A.; FitzGerald, S.; El-Sayed, M. A.; Schaff, T. G.; Whetten, R. L. Visible to Infrared Luminescence from a 28-atom Gold Cluster. J. Phys. Chem. B 2002, 106, 3410-3415.

[25] Wen, X.; Yu, P.; Toh, Y. R.; Tang, J. Strucute-correlated Dual Fluorescent Bands in BSA-protected Au_{25} Nanoclusters. J. Phys. Chem. C 2012, 116, 11830-11836.

[26] Wu, Z.; Jin, R. On the Ligand's Role in the Fluorescence of Gold Nanoclusters. Nano Lett. 2010, 10, 2568–2573.

[27] Pakiari, A. H.; Jamshidi, Z. Nature and Strength of M-S Bonds (M = Au, Ag, and Cu) in Binary Alloy Gold Clusters. J. Phys. Chem. A 2010, 114, 9212–9221.

[28] Bau, R. Crystal Structure of the Antiarthritic Drug Gold Thiomalate (Myochrysine): A Double-Helical Geometry in the Solid State. J. Am. Chem. Soc. 1998, 120, 9380-9381.

[29] Odriozola, I.; Loinaz, I.; Pomposo J. A.; Grande, H. J. Gold–Glutathione Supramolecular Hydrogels. J. Mater. Chem., 2007, 17, 4843–4845

[30] Hammouda, B. A new Guinier–Porod model. J. Appl. Cryst. 2010, 43, 716-719.

[31] Liu, R.-F.; Franzese, C. A.; Malek, R.; Żuchowski, P. S.; Ángyán, J. G.; Szczęśniak, M. M.; Chazasiński, G. Aurophilic Interactions from Wave Function, Symmetry-Adapted Perturbation Theory, and Rangehybrid Approaches. J. Chem. Theory Comput. 2011, 7, 2399–2407.

[32] Söptei, B.; Mihály, J.; Visy, J.; Wacha, A.; Bóta, A. Intercalation of Bovine Serum Albumin Coated Gold Clusters Between Phospholipid Bilayers: Temperature Dependent Behavior of Lipid-AuQC@BSA Assemblies with Red Emission and Superlattice Structure. J. Phys. Chem. B 2014, 118, 3887-3892.

[33] Smith, W. E.; Reglinski, J.; Hoey, S.; Brown, D. H.; Sturrock, R. D. Action of Sodium Gold(I) Thiomalate on Erythrocyte Membrane. Inorg. Chem. 1990, 29, 5190-5196.

[34] Irwin, M. J.; Vittal, J. J.; Puddhepatt, R. J. Luminescent Gold(I) Acetylides: From Model Compounds to Polymers. Organometallics 1997, 16, 3541-3547.

[35] Zhang, J.; Chi, Q.; Nielsen, J. U.; Friis, E. P.; Andersen, J. E. T.; Ulstrup, J. Two-Dimensional Cysteine and Cystine Cluster Networks on Au(111) Disclosed by Voltammetry and in Situ Scanning Tunneling Microscopy. Langmuir 2000, 16, 7229-7237.

[36] T. R. Ralph, M. L. Hitchman, J. P. Millington, F. C. Walsh, J. Electroanal. Chem. 375, 1, (1994) Issues 1–2, 19 September 1994, Pages 1–15. The Electrochemistry of L-Cystine and L-Cysteine: Part 1: Thermodynamic and Kinetic Studies

[37] Mink, J.; Hajba, L.; Mihály, J.; Németh, Cs.; Pálmai M.; Sandström, M. Vibrational Spectroscopic Studies of Molecules with Biochemical Interest: The Cysteine Zwitterion. Appl. Spectrosc. Rev. 2012, 47, 415-483

[38] Parker, S. F. Assignment of the Vibrational Spectrum of L-Cysteine. Chemical Physics 2013, 424, 75-79

[39] Quian, W.; Krimm, S. Conformation Dependence of the SH and CS Stretch Frequencies of the Cysteine Residue

[40] Lewies, R. N. A. H.; McElhaney, R. N.; Pohle, W.; Mantsch, H. H. Components of the Carbonyl Stretching Band in the Infrared Spectra of Hydrated 1,2-Diacykglycerol Bilayers: A Reevaluation. Biophys. J. 1994, 67, 2367−2375.

[41] Mocanua, A.; Cernicab, I.; Tomoaiac, G.; Bobosa, L.-D.; Horovitz, O.; Tomoaia-Cotisel, M. Self-assembly characteristics of gold nanoparticles in the presence of cysteine. Colloids and Surfaces A: Physicochem. Eng. Aspects 2009, 338, 93–101